J. Fluid Mech. (1988), *vol.* 197, *pp.* 479–501
Printed in Great Britain

Bifurcation phenomena in Taylor–Couette flow with buoyancy effects

By K. S. BALL† AND B. FAROUK‡

† Division of Applied Mathematics, Brown University, Providence, RI 02912, USA

‡ Department of Mechanical Engineering and Mechanics, Drexel University, Philadelphia, PA 19104, USA

(Received 14 August 1987 and in revised form 30 May 1988)

A numerical study has been conducted to determine the various modes of Taylor–Couette flow that exist between concentric vertical cylinders, as the aspect ratio Γ (height to gap width, H/d) and the Reynolds number Re (based on the inner cylinder speed) are varied. Furthermore, the effects of the introduction of buoyancy on the development of the flow are examined. This is accomplished by considering both cylinders to be isothermal, with the rotating inner cylinder at a higher temperature than the stationary outer cylinder. Results are presented for a wide range of the Grashof number Gr (based on the temperature difference ΔT across the annular gap). The structure of the Taylor vortices is observed to be distorted considerably with the buoyant flows, and the nature of the onset and subsequent development of the vortices is altered. The hysteresis between the different modes of cellular flow, characteristic of the bifurcation phenomena, is also substantially modified.

1. Introduction

The bifurcation phenomena occurring in the Taylor problem have been examined in great detail during the last ten years (a good review of the general Taylor problem can be found in DiPrima & Swinney 1985). In the idealized model of Taylor–Couette flow, where the annulus is infinitely long, periodic flows arise from symmetric supercritical bifurcations in the circular Couette-flow solution. With realistic (finite) end conditions, however, the symmetry of the bifurcations is broken. In an attempt to improve upon the inadequacy of the idealized model, Benjamin (1978*a*) used the abstract mathematical theory of Leray-Schauder to include the end effects associated with a finite-length annulus in his analysis of the Taylor problem. Benjamin considered the dependence of the flow on two parameters, one the Reynolds number Re and the other the (non-dimensional) height Γ of the annulus. He predicted the existence of a hysteresis of the primary-flow locus, which accompanies the morphogenesis of the cellular structure as Re is varied through critical values of Γ.

The various modes of cellular flow are characterized by the number of Taylor cells present. For a particular range of Γ, a unique mode with an even number of cells emerges as the primary flow as the speed of the inner cylinder is gradually increased from rest. Other cellular flows are also realizable as secondary modes, at values of Γ for which another flow is primary. These flows are only stable at values of Re larger than the critical value of Re for the development of the primary flow from the resting state. These secondary modes can be achieved by giving the system an impulsive

start to the desired speed of rotation. As the rotational speed is subsequently decreased, a critical value of Re is reached where the secondary mode collapses catastrophically into the primary mode. The form of this exchange between the primary and secondary modes is characterized by a cusp in the (Re, Γ)-control plane.

In a series of accompanying experiments, Benjamin (1978*b*) was able to verify his theoretical predictions. Using a Taylor apparatus with a radius ratio of $\eta = 0.615$, Benjamin varied the aspect ratio Γ over the range $3.4 < \Gamma < 4.0$. At the lower values of this range, two Taylor cells were observed to develop as the Reynolds number was gradually increased from rest, while four cells developed at the upper values. The exchange of priorities between the two-cell state and the four-cell state as the primary flow occurs in this range, and the locus of critical values for the stability of the two flows was found to be a downward-facing cusp in the (Re, Γ)-plane.

Schaeffer (1980) proposed a model problem to study analytically the boundary effects and bifurcation phenomena observed by Benjamin. Hall (1980, 1982) extended Schaeffer's analysis by using perturbation methods, and verified that the model can predict the form of the exchange between the primary and secondary modes. In particular, Hall was able to predict the form of the exchange of stability between the four-cell and six-cell states, namely, an upward-facing cusp.

In a subsequent series of experiments, Mullin, Pfister & Lorenzen (1982) and Mullin (1982) extended Benjamin's findings to higher values of Γ, covering the exchange of priorities between the four-cell state and the six-cell state. As predicted by Hall, the stability locus was found to be an upward-facing cusp. Mullin also presented results for the 6–8, 8–10, and 10–12 cell transitions occurring at increasingly higher values of the aspect ratio, which were broadly in accord with the ideas proposed by Benjamin.

An essential factor in the primary-flow exchange process is the multiplicity of distinct steady flows, all of which can exist on the same boundary conditions. Benjamin & Mullin (1981) present experimental observations of many of these secondary modes, in the context of their earlier works. Some of the possible flows observed in the studies dealing with the multiplicity of the Taylor-cell states have been termed anomalous modes, since they can only occur at sufficiently high Reynolds numbers and always collapse as Re is gradually reduced. These steady, secondary states are characterized by a direction of rotation opposite to that of the stable flows occurring at lower Re; namely, the flow adjacent to the ends is in the outward direction (from the inner cylinder towards the outer cylinder). The jet-like flow structure occurring between the pairs of cells is consequently an inward flow, which is opposite to the normal Taylor-cell states. Frequently, the total number of cells in an anomalous mode is odd. Cliffe (1983) complemented these experimental results by presenting numerical solutions for these flows at small aspect ratios.

Anomalous modes were first observed in relatively short annuli. However, these effects are intrinsic to the hydrodynamic stability problem, and can be expected to be important in any Taylor apparatus, no matter how long it is. Benjamin & Mullin (1982) presented further experimental results, showing as many as twenty different stable steady flows in a moderately long Taylor apparatus. Lorenzen & Mullin (1985) obtained experimental evidence of up to forty anomalous cells, and concluded that the finite length of the annulus plays a crucial role in determining the overall stability of the flow. Hughes *et al.* (1985) were able to successfully predict a variety of these secondary flows using a finite-difference method. However, they did not investigate the hysteresis phenomenon predicted and observed by Benjamin. Cliffe

& Mullin (1985) also performed numerical calculations of the anomalous modes, and their predictions compared favourably with new experimental data, which they also presented.

The first numerical predictions of the hysteresis effects predicted by Benjamin (1978*a*) and observed by Mullin (1982) were presented by Jones & Cliffe (1983). They studied the exchange process between a four-cell and a six-cell flow, by utilizing the finite-element method together with continuation methods designed especially for tracking bifurcating solutions. They also performed a limited number of finite-difference calculations to confirm their results at selected parameter values. They obtained substantial agreement with the experimental results of Mullin (1982). Cliffe (1988) extended this work to include the two–four cell exchange, and also provided a detailed study of the stability of those solutions.

In all of these previous studies, the flows considered were isothermal. The influence of buoyancy on the behaviour of the Taylor–Couette flow was not studied. However, rotating flows which are not isothermal occur in a variety of technological applications, such as the cooling of conventional rotating machinery (Krieth 1968) or chemical vapour deposition (CVD) processes (Bettes 1982; Singer 1984; Bollen 1978). Buoyant rotating flows also have many geophysical applications, including oceanic and atmospheric circulation, and hence play important roles in developing weather patterns (Greenspan 1968).

In spite of their technological importance, comparatively little work has been directed toward the study of the mixed convection flows within rotating cylindrical annuli. The first attenpts to study this problem were primarily experimental, and were usually coupled with an axial flow through the annular gap. The primary thrust of these early studies was to determine the overall heat transfer rates across the annular gap, and little information regarding the hydrodynamic stability of the flows was given (Kaye & Elgar 1958; Gazley 1958; Bjorklund & Kays 1959; Becker & Kaye 1962*a*).

Later theoretical studies focused on the stability of the circular Couette flow in the presence of a radial temperature gradient (Becker & Kaye 1982*b*; Walowit, Tsao & DiPrima 1964; Fung & Kurzweg 1975). With the inner cylinder rotating, it was concluded that a positive gradient of temperature across the annular gap (i.e. a heated outer cylinder and a cooled inner cylinder) is destabilizing, while a negative temperature gradient is stabilizing. This can be explained by noting that a greater centrifugal force is exerted on a heavier (cooler) fluid particle. Thus, fluid particles adjacent to a cooled inner cylinder would have a greater tendency to be displaced by the rotating flow. In these analyses, the gravity force (buoyancy) was neglected. Walowit *et al.* (1964) justified this seemingly severe restriction by noting that in the conduction regime ($Gr \leqslant 10^3$), natural convection has little effect on the heat transfer, and can therefore be expected to have little effect on the stability of the flow. However, Snyder & Karlsson (1964) concluded that the axial flow induced by buoyancy does, in fact, have a significant influence on the stability of the flow. They found that both positive and negative radial gradients of temperature are stabilizing, provided that the magnitude of ΔT is small. For larger ΔT, a spiral form of instability was observed (see also Snyder 1965 and Karlsson & Snyder 1965). More recent experimental studies have also confirmed the stabilizing effects of a positive density gradient (Withjack & Chen 1974; Gardiner & Sabersky 1978).

It should be mentioned that spiral solutions can occur in other configurations of the Taylor apparatus, notably in systems with an axial flow superimposed and in systems with both cylinders rotating. For the first configuration, see for example

Astill (1964) or more recently Wan & Coney (1982). The latter case is currently being investigated by a number of researchers. Andereck, Liu & Swinney (1986) conducted extensive experiments with independently rotating cylinders, and have mapped the 18 principal flow regimes they observed while varying the inner- and outer-cylinder Reynolds numbers. In a theoretical study using bifurcation theory, Chossat, Demay & Iooss (1985) found spiral solutions resulting from symmetry-breaking bifurcations, which are consistent with the experimental results cited above (see also Demay & Iooss 1984 and Chossat & Iooss 1985).

Only recently have any numerical studies been reported in the literature for the mixed convection flows in a rotating annulus. Leonardi, Reizes & de Vahl Davis (1982) and de Vahl Davis, Leonard & Reizes (1984) presented the results of finite-difference calculations for axisymmetric, vertical annuli with short to moderate aspect ratios. A taller annulus was considered by Ball & Farouk (1986, 1987). These studies concentrated on the overall flow patterns and heat transfer rates. No detailed information regarding flow bifurcation was given, although some results regarding the development of the secondary flow and its effects on the heat transfer mechanism were given by Ball & Farouk (1987).

While there are numerous results available for the hydrodynamic stability of the isothermal flows, the mutual interactions between both the buoyancy and rotational forces and the subsequent effects on the stability of the flows has yet to be adequately treated and fully described. The present study is a step in this direction (see also Ball 1987).

2. Mathematical formulation

The geometry considered consists of a smooth, heated isothermal vertical cylinder of radius R_i enclosed by a concentric isothermal cylinder of radius R_o to form an annulus. The annulus is capped by smooth, adiabatic horizontal endplates. Both the outer cylinder and the endplates are fixed and stationary, while the inner cylinder rotates with an angular velocity Ω. The geometry is specified by the radius ratio $\eta = R_i/R_o$ and the aspect ratio $\Gamma = H/d$, where d is the gap width $R_o - R_i$. The problem geometry is shown in figure 1. It is noted that the inner cylinder will always be on the right for all results presented in this paper.

The fluid considered is air, with a Prandtl number of $Pr = 0.7$ (where $Pr = \nu/\alpha$, the ratio of the kinematic viscosity of the fluid to its thermal diffusivity). The usual Boussinesq approximation is applied. The Boussinesq approximation remains valid in rotating flows when the centrifugally induced pressure difference effects on the density may be neglected. The criterion used to determine this is that the acceleration ratio A, defined as the ratio of the characteristic centrifugal acceleration to the acceleration due to gravity, should be small compared with unity: $A = (\Omega^2 R_i)/g \ll 1$. For all results presented, $A < 0.03$.

In the mixed convection system, the regions of stability of the resulting flows are quantified in terms of the Grashof number $Gr = g\beta\Delta T d^3/\nu^2$ (where β is the volumetric coefficient of thermal expansion) and the Reynolds number $Re = (R_i\,\Omega)\,d/\nu$. The Grashof number characterizes the buoyancy force, while the Reynolds number characterizes the rotational (centrifugal) force. Of particular interest is the ratio Gr/Re^2, denoted by σ, which indicates the relative importance of the buoyancy and rotational effects. This parameter can be determined from an order-of-magnitude analysis of the governing equations for mixed convection flows (cf. Holman 1981). For values of σ near unity, the two forces are of similar magnitude.

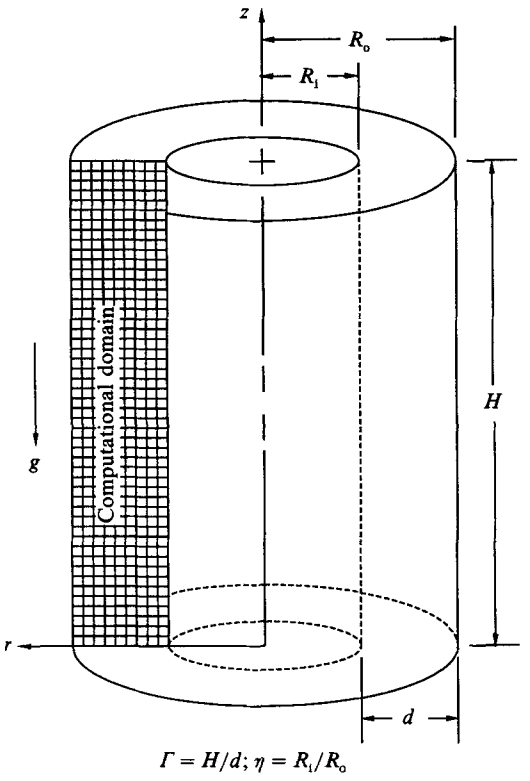

FIGURE 1. Problem geometry.

The flows under consideration are assumed to be axisymmetric over a wide range of both the Reynolds and Grashof numbers, and are therefore readily accessible to numerical solution. Snyder and Karlsson presented experimental observations for the small-gap annulus ($d = 0.267$ cm, with $2d/(R_i + R_o) \ll 1$) with a radial thermal gradient imposed upon the flow (Snyder & Karlsson 1964; Snyder 1965; Karlsson & Snyder 1965). They reported that a spiral form of the Taylor-vortex flow occurs when the gradient across the gap, $\Delta T/d$, exceeds ± 5 °C/cm. In the present study, the thermal gradients considered were of the order of 1 °C/cm across the 5 cm gap, and it is expected that these flows will also remain axisymmetric. This assumption was largely corroborated by the flow-visualization studies discussed in Ball (1987), where the spiral mode of flow was observed to occur over an extremely small range of the rotational parameter σ (approximately $0.3 > \sigma > 0.1$).

2.1. *Governing equations*

The Navier–Stokes and energy equations, together with the continuity equation, completely describe the physics of the problem. In cylindrical polar coordinates, for an axisymmetric flow, the equations are

$$\frac{\partial u}{\partial t} + u\frac{\partial u}{\partial r} + w\frac{\partial u}{\partial z} - \frac{v^2}{r} = -\frac{1}{\rho_0}\frac{\partial p}{\partial r} + \nu\left(\frac{\partial^2 u}{\partial r^2} + \frac{1}{r}\frac{\partial u}{\partial r} - \frac{u}{r^2} + \frac{\partial^2 u}{\partial z^2}\right), \tag{1}$$

$$\frac{\partial v}{\partial t} + u\frac{\partial v}{\partial t} + w\frac{\partial v}{\partial z} + \frac{uv}{r} = \nu\left(\frac{\partial^2 v}{\partial r^2} + \frac{1}{r}\frac{\partial v}{\partial r} - \frac{v}{r^2} + \frac{\partial^2 v}{\partial z^2}\right), \tag{2}$$

$$\frac{\partial w}{\partial t}+u\frac{\partial w}{\partial r}+w\frac{\partial w}{\partial z}=-\frac{1}{\rho_0}\frac{\partial p}{\partial z}+\nu\left(\frac{\partial^2 w}{\partial r^2}+\frac{1}{r}\frac{\partial w}{\partial r}+\frac{\partial^2 w}{\partial z^2}\right)+g\beta(T-T_0), \tag{3}$$

$$\frac{\partial T}{\partial t}+u\frac{\partial T}{\partial r}+w\frac{\partial T}{\partial z}=\alpha\left(\frac{\partial^2 T}{\partial r^2}+\frac{1}{r}\frac{\partial T}{\partial r}+\frac{\partial^2 T}{\partial z^2}\right), \tag{4}$$

$$\frac{\partial u}{\partial r}+\frac{u}{r}+\frac{\partial w}{\partial z}=0. \tag{5}$$

These equations are transformed into the stream function–vorticity form by intoducing the stream function ψ and vorticity ω as follows:

$$u=-\frac{1}{\rho r}\frac{\partial \psi}{\partial z};\quad w=\frac{1}{\rho r}\frac{\partial \psi}{\partial r}, \tag{6}$$

$$\omega=\frac{\partial u}{\partial z}-\frac{\partial w}{\partial r}. \tag{7}$$

The equations are made dimensionless by using the gap width d as the lengthscale, d^2/ν as the timescale, and the temperature difference (T_i-T_0). The resulting system of coupled, elliptic equations to be solved is

$$\frac{\partial}{\partial r}\left(\frac{1}{r}\frac{\partial \psi}{\partial r}\right)+\frac{\partial}{\partial z}\left(\frac{1}{r}\frac{\partial \psi}{\partial z}\right)=-\omega, \tag{8}$$

$$\frac{\partial \omega}{\partial t}-\frac{\partial}{\partial r}\left(\frac{\omega}{r}\frac{\partial \psi}{\partial z}\right)+\frac{\partial}{\partial z}\left(\frac{\omega}{r}\frac{\partial \psi}{\partial r}\right)-\frac{\partial}{\partial z}\left(\frac{v^2}{r}\right)=-Gr\frac{\partial T}{\partial r}+\frac{\partial^2 \omega}{\partial r^2}+\frac{1}{r}\frac{\partial \omega}{\partial r}-\frac{\omega}{r^2}+\frac{\partial^2 \omega}{\partial z^2}, \tag{9}$$

$$\frac{\partial v}{\partial t}-\frac{\partial}{\partial r}\left(\frac{v}{r}\frac{\partial \psi}{\partial z}\right)+\frac{\partial}{\partial z}\left(\frac{v}{r}\frac{\partial \psi}{\partial r}\right)-2\frac{v}{r^2}\frac{\partial \psi}{\partial z}=\frac{\partial^2 v}{\partial r^2}+\frac{1}{r}\frac{\partial v}{\partial r}-\frac{v}{r^2}+\frac{\partial^2 v}{\partial z^2}, \tag{10}$$

$$\frac{\partial T}{\partial t}-\frac{1}{r}\frac{\partial}{\partial r}\left(T\frac{\partial \psi}{\partial z}\right)+\frac{1}{r}\frac{\partial}{\partial z}\left(T\frac{\partial \psi}{\partial r}\right)=\frac{1}{Pr}\left(\frac{\partial^2 T}{\partial r^2}+\frac{1}{r}\frac{\partial T}{\partial r}+\frac{\partial^2 T}{\partial z^2}\right). \tag{11}$$

2.2. *Boundary conditions*

The value of the stream function ψ along all boundaries must be a constant, due to the no-slip condition at an impermeable wall. This value was taken to be zero. The swirl-velocity component is equal to zero at both the endplates and the outer cylinder, which are stationary. The inner cylinder rotates with an angular speed Ω, so the non-dimensional swirl velocity there becomes the Reynolds number Re. It is noted that the corners of the computational domain do not enter the calculations in the discretization scheme chosen. Therefore, no problems are encountered with any discontinuities in the boundary conditions.

An expression for the vorticity boundary condition can be obtained by expanding the stream function near the surface using a three-term Taylor series expansion and by making use of the continuity and no-slip conditions: $\omega=-2.0\psi_{nw}/(\Delta n)^2/r_w$, where ψ_{nw} is the value of ψ at the near-wall node (adjacent to the wall), Δn is the non-dimensional distance of the near-wall node from the wall, and r_w is the value of the normal coordinate at the wall node being calculated. Finally, the non-dimensional temperature at the inner wall is $T=1$ and at the outer wall $T=0$, with both endplates taken to be adiabatic.

2.3. *Solution procedure*

The resulting four coupled elliptic equations (for stream function, vorticity, swirl velocity, and temperature) are discretized by using a control-volume based finite-difference method (for a discussion of the control-volume method, see for example Gosman *et al.* 1969). A line-by-line tridiagonal matrix algorithm is used together with a successive substitution technique to solve the finite-difference equations along with the prescribed boundary conditions. A fully implicit scheme was used to obtain the transient solutions, and the convective–diffusive terms were discretized using a hybrid method (Patankar 1980).

In this study, 21 grid points were used in the radial direction, while the number of grid points in the axial direction was varied with the changing aspect ratio Γ so that a minimum density of 12Γ points was maintained. A grid independence study was used to determine the smallest possible grid size that would still produce accurate solutions. An additional check on the grid size was made by computing the grid Péclet numbers Pe for several 'worst case' runs (where the Péclet number is defined as the ratio of the convection to diffusion terms, cf. Patankar 1980). In these cases, all but a very few (less than 5%) of the nodal points had grid Péclet-number values of less than two. Of those that were higher than two, none exceeded $Pe = 3.0$. Thus, for all intents and purposes, the hybrid scheme was reduced to a central-difference scheme. All computations were performed on a CRAY X-MP super-computer.

3. Results

In the present study, two sets of results will be considered, with $\eta = 0.5$ in both cases. The first results examined will be those for the two-cell to four-cell transition occurring for small values of the aspect ratio Γ, and the second results presented are for the four-cell to six-cell transition occurring in the range of aspect ratio where $\Gamma > 4.2$. In both cases, the isothermal results will be discussed first and compared to the available previous studies. Then, new results showing the effect of the buoyancy forces will be discussed, highlighting the differences in the nature of the exchange process and the transitions to different modes of flow.

It is noted that the Prandtl number only becomes a parameter of the mixed convection system through the energy equation, (11). Thus, even though the previous studies were not conducted in air, comparisons with those isothermal results should not be affected by the differing values of Pr encountered. Prandtl-number effects on the buoyant flows will not be considered in this paper.

3.1. *The two-cell to four-cell transition*

The purpose of the first series of computations was to determine the primary flow locus for the isothermal flow, so that a comparison with the experimental results presented by Benjamin (1978*b*) for the bifurcation set in the (Re, Γ)-plane for two-cell and four-cell flows could be made. In this way, the procedure used and the accuracy of the results obtained could be verified. It was especially desired to predict the qualitative nature of the exchange, as determined from the shape of the primary-flow locus. A close quantitative agreement was not expected since the radius ratio used in this study ($\eta = 0.5$) is different from that used by Benjamin ($\eta = 0.615$).

In figure 2, the experimental results of Benjamin have been reproduced, and are compared with the finite-difference predictions made in this study. To generate the

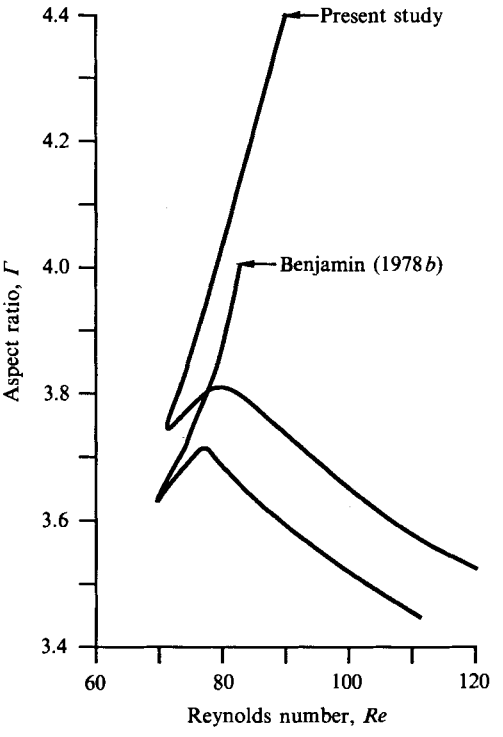

FIGURE 2. Bifurcation set for the isothermal ($Gr = 0$) two-cell and four-cell flows.

primary-flow locus numerically, the following procedure was used. First, the bottom portion of the locus was determined by a series of impulsive runs, in which the initial values of all variables throughout the entire computational domain were set equal to zero. The single exception to this, of course, was at the boundary of the inner cylinder, which corresponded to the desired Reynolds number. If the steady-state results obtained from an impulsive start at any particular values of Γ and Re consisted of two cells, then Re was increased and the run was repeated. Conversely, if the steady-state results consisted of four cells, Re was decreased and the run was repeated. Eventually, the critical value of the Reynolds number was determined through this iterative procedure. The maximum increment or decrement in Re used to determine the critical value was ± 5. As the critical value was approached, a limit-cycle behaviour was observed, where the time required to reach the steady state increased dramatically. This behaviour was also noted by Jones & Cliffe (1983).

Once the lower portion of the locus was determined, the upper part was found by gradually increasing the aspect ratio Γ at fixed values of the Reynolds number Re. The calculations were started using the results of the two-cell solution found at values of Γ just below the lower part of the locus, and Γ was increased in intervals of 0.05. At all stages, the solution from the neighbouring (lower) value of Γ was used as the initial values for the next computation, which was allowed to proceed until a steady-state solution was obtained. This technique, the quasi-static variation of parameters, was also used by Jones & Cliffe (1983). It is a crude continuation method, but is easily implemented using finite-difference codes. Runs were continued with increasing Γ until the collapse of the steady two-cell state was observed, after which either a steady four-cell state emerged or a limit-cycle behaviour was encountered.

Using these methods, the determination of the loci required a considerable number of computational runs. While the minimum number of runs required to determine any single point on the bottom portion of each locus was two, in practice four or five runs were required to accurately determine each critical point. Many more runs were then required as the aspect ratio was increased in gradual increments to find the upper portion of each locus. Consequently, the use of a supercomputer (CRAY X-MP) was essential in obtaining the results in a reasonable amount of time.

As described above, two different methods were used to determine the critical points. The impulsive-run method was used to determine the lower portion of each locus, because it generally required a smaller number of runs to determine each point, and the convergence of each individual run was much faster compared with the quasi-static runs. These two factors resulted in a significant savings of CPU time. However, the impulsive-run technique could not be used to find the secondary flows above the aspect ratio corresponding to the transcritical bifurcation point. In these cases, the primary flow always emerged as the steady-state solution, no matter how large the value of the Reynolds number. Thus, the quasi-static variation of Γ at fixed Re was the only alternative for locating the critical points along the upper portion of the locus. It is noted that this behaviour was also observed in the experiments of Benjamin and Mullin.

As shown in figure 2, an excellent qualitative agreement with Benjamin's data was obtained. In particular, the shape and extent of the cusp is identical to Benjamin's. Quantitatively, though, the numerically generated cusp is shifted towards higher values of Γ. The upward shift in Γ represents an increase in the stability of the two-cell flow at the expense of the four-cell flow. This is consistent with a decrease in the radius ratio η (recall that $\eta = 0.5$ in this study compared with $\eta = 0.615$ in Benjamin's), since the change in the dimensionless wavenumber k from $\eta = 0.615$ to $\eta = 0.5$ is less than 1% (Walowit *et al.* 1964). Thus, since k is non-dimensionalized by the gap width, the relatively larger gap width in the numerical study favours the development of the larger cell size in the short annulus.

For the isothermal flow, the cusp is pointing obliquely downward. The flow at values of Re just to the left of this cusp comprises a weakened four-cell flow, which is recognized as a rudimentary version of the four-cell flow possible at higher-values of Re at the same aspect ratio. After this weak four-cell flow is established, very gradual increases in Re to the right of the cusp result in the appearance of a two-cell flow. With further increases in Re, a fully developed four-cell flow re-emerges. The 4–2–4 progression of cell states with increasing Re at $\Gamma = 3.8$ is shown in figure 3.

In figure 4, the effects of adding buoyancy to the system by heating the inner cylinders are examined. Shown in this figure are the loci for three fixed values of the Grashof number (the numerically generated isothermal flow locus is reproduced in figure 4 to facilitate comparisons with the buoyant flow loci). It is observed that even a relatively small amount of buoyancy has a surprisingly significant effect on the behaviour of the flow and its exchange process, and the nature of the cusp has been totally changed.

These results can be explained in terms of an unfolding of the pitchfork bifurcation, which arises from imperfections in the system. To demonstrate this, an analogy is made with an unfolding of codimension 2:

$$G(x, \lambda, \alpha) = x^3 - \lambda x + \alpha_1 + \alpha_2 x^2.$$

α_1 and α_2 are functions of the imperfections, in this case the aspect ratio Γ and the buoyancy parameter Gr (the Reynolds number is represented by λ, the bifurcation

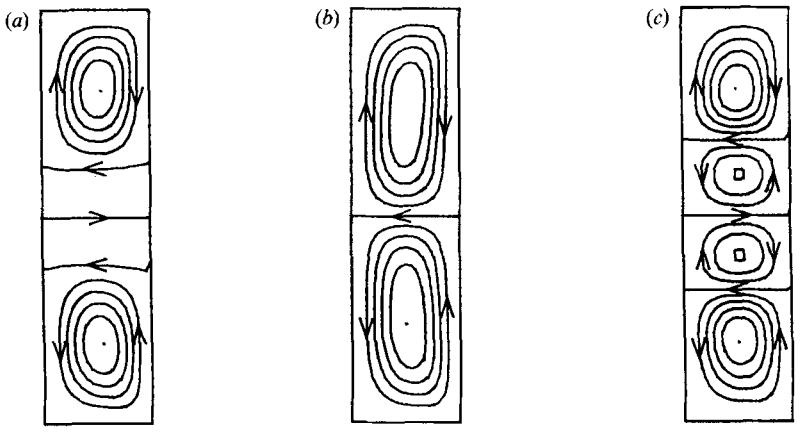

FIGURE 3. 4–2–4 Flow transition with increasing Re at $\Gamma = 3.8$, with $Gr = 0$, (a) $Re = 70$, (b) 80, (c) 85.

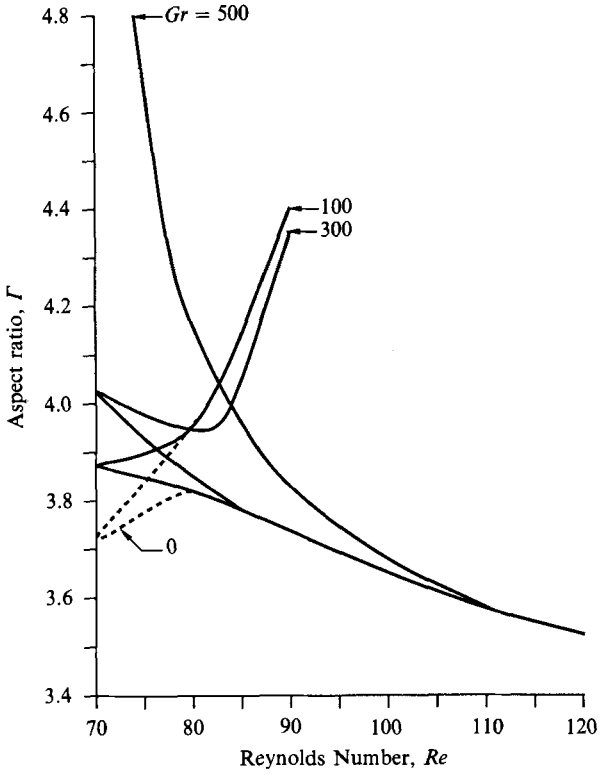

FIGURE 4. Bifurcation set for the buoyant two-cell and four-cell flows.

parameter). The state variable x can be any functional of the solution which discriminates between the different solution states (characterized by the number of Taylor cells). For example, Jones & Cliffe (1983) and Cliffe (1984) chose the radial velocity at the centre of the annulus as the state variable.

According to Golubitsky & Schaeffer (1985), there are essentially four different bifurcation diagrams that can occur as α varies. These are shown in figure 5, where the (α_1, α_2)-plane is divided into four regions by the two curves $\alpha_1 = 0$ and

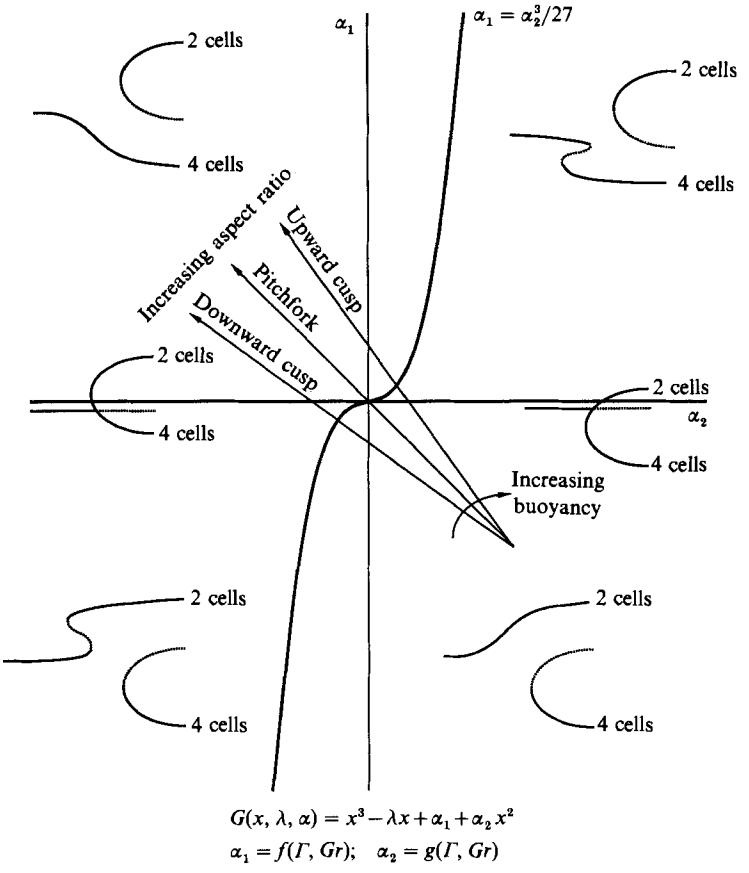

FIGURE 5. Unfolding of the pitchfork bifurcation: 2–4 cell exchange of priorities.

$\alpha_1 = \alpha_2^3/27$. Along the curve $\alpha_1 = 0$, transcritical bifurcations are encountered, while hysteresis points are found along the curve $\alpha_1 = \alpha_2^3/27$. At the origin, where the imperfections in the system disappear, the symmetric pitchfork bifurcation is recovered.

For the two-cell to four-cell transition, at sufficiently low values of Γ, the two-cell flow emerges as the primary flow upon a gradual increase in Re. This is represented by the bifurcation diagram in the lower right corner of figure 5 (where $\alpha_1 < 0$ and $\alpha_2^3 > 27\alpha_1$). On the other hand, a four-cell flow emerges as the primary flow at sufficiently high values of Γ. This is represented by the bifurcation diagram in the upper left corner of figure 5 ($\alpha_1 > 0$ and $\alpha_2^3 < 27\alpha_1$).

The orientation of the cusp observed in the (Re, Γ)-plane depends upon the path taken in the (α_1, α_2)-plane between these two regions. For a downward-facing cusp, the hysteresis point occurs at a lower value of Γ than the transcritical bifurcation. Therefore, the curve followed in the (α_1, α_2)-plane with increasing Γ must pass to the left of the origin. By similar reasoning, the curve in the (α_1, α_2)-plane representing the upward facing cusp must pass to the right of the origin. It is reasonable to assume that the unfolding of the pitchfork bifurcation is continuous in the auxiliary parameters α. Therefore, a pitchfork bifurcation must occur as the cusp changes its orientation from downward-facing to upward-facing with increasing Gr, and is represented by a curve in the (α_1, α_2)-plane passing through the origin. This is also

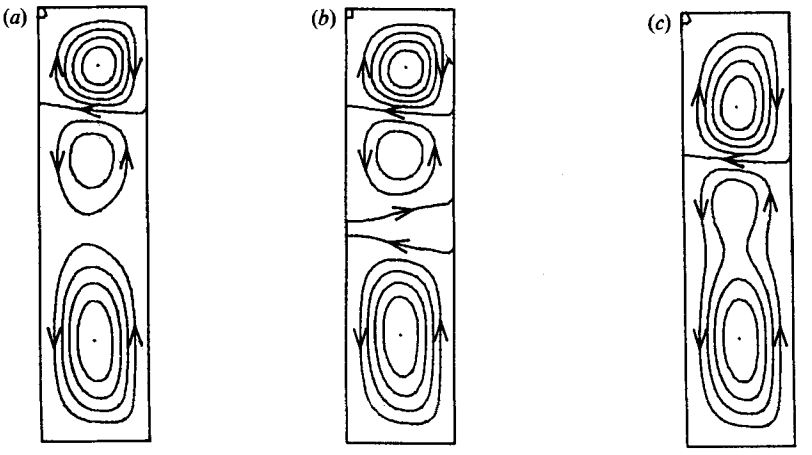

FIGURE 6. 2–4–2 Flow transition with increasing Re at $\Gamma = 4.0$, with $Gr = 300$, (*a*) $Re = 70$, (*b*) 75, (*c*) 85.

shown in figure 5, together with the effects of increasing buoyancy (given by Gr) in the system.

For the flows with $Gr = 100$, the weakened version of the four-cell flow was never observed. The presence of buoyancy forces has completely eliminated this mode of flow, and the cusp has become aligned with the Re-axis, indicating a pitchfork bifurcation. The physical explanation offered is that the weak, negative Taylor cell (the second cell up from the bottom in figure 3*a*) was not strong enough to force the buoyant flow adjacent to the heated cylinder to flow in the downward direction. For the sake of clarity in this discussion, a vortex will be considered to have a positive sense when its rotation is in the same sense as the natural convection flow, viz. when the flow immediately adjacent to the heated inner cylinder is in the upward (positive z) direction. This effect is further enhanced as the Grashof number is increased, as shown in figure 4 where the exchange process is now characterized by an upward-pointing cusp. Thus, the hysteresis for the buoyant flows is from a two-cell flow to a four-cell flow, and then back to a two-cell flow. The 2–4–2 progression of cell states with increasing Re at $\Gamma = 4.0$, with $Gr = 300$, is shown in figure 6. As the increase in the Grashof number is continued, the primary two-cell flow dominates the system, and by the time $Gr = 500$, the cusp is no longer observable in this range of Γ. Indeed, there is no indication that any hysteresis effects remain at all.

Another striking difference between the buoyant two-to-four cell transition and its isothermal counterpart is the range of Γ over which the transition occurs at fixed values of Re. In the isothermal flows, this transition is always very abrupt. By contrast, the transition is very gradual in the buoyant flows, with an intermediate form occurring prior to the complete onset of the four-cell mode at lower values of Re. This gradual transition is shown in figure 7, where $Gr = 300$ and $Re = 70$. The intermediate form is characterized by a relatively large stagnant region, where a negative Taylor cell is slowly forming on the inner wall of the cylinder. For the purposes of determining the stability locus, the first sign of this negative involution was used as the stability criterion.

The last two figures presented in this section contrast the transient nature of the two-to-four cell transition in the isothermal and mixed convection flow situations. In figure 8, the loss of stability of the two-cell flow is shown at $Re = 85$ and $\Gamma = 4.2$, where the solution from $\Gamma = 4.15$ was used for the initial values of the calculation.

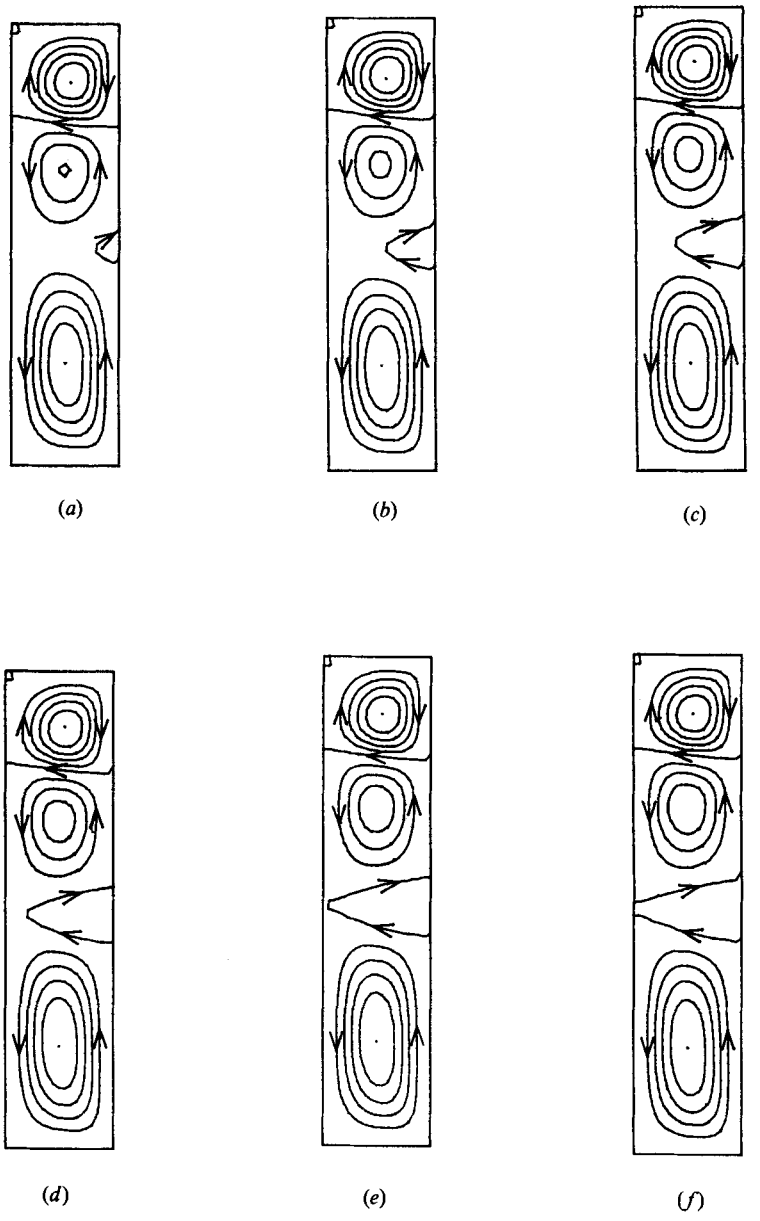

FIGURE 7. Two-to-four cell transition for buoyant flows with increasing Γ, at $Re = 70$ and $Gr = 300$, (*a*) $\Gamma = 4.1$, (*b*) 4.2, (*c*) 4.3, (*d*) 4.4, (*e*) 4.5, (*f*) 4.6.

It is observed that the development of the new pair of cells is symmetric about the midplane, and occurs near the interface between the two counter-rotating cells.

By contrast, the two-to-four cell transition for the buoyant flows occurs by an involution of the positive cell, as shown in figure 9. This trait has been generally observed in all of the buoyant flows considered. The positive cells have a greater tendency to increase in size as the aspect ratio increases, and as they get longer, they become weaker near the bottom. After a certain point, the flow stagnates, allowing the negative Taylor cell to encroach upon it, eventually splitting it in two to form the extra pair of cells. This phenomenon is further explained in the next section.

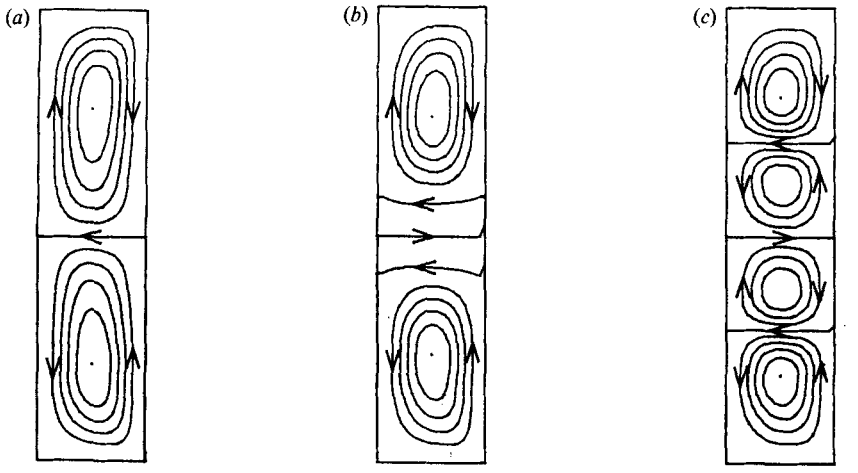

FIGURE 8. Transient development of 2–4 transition for isothermal flows, at $Re = 85$ and $\Gamma = 4.2$ (Fourier number $Fo = tv/d^2$), (a) $Fo = 0$, (b) 6.19, (c) 12.37.

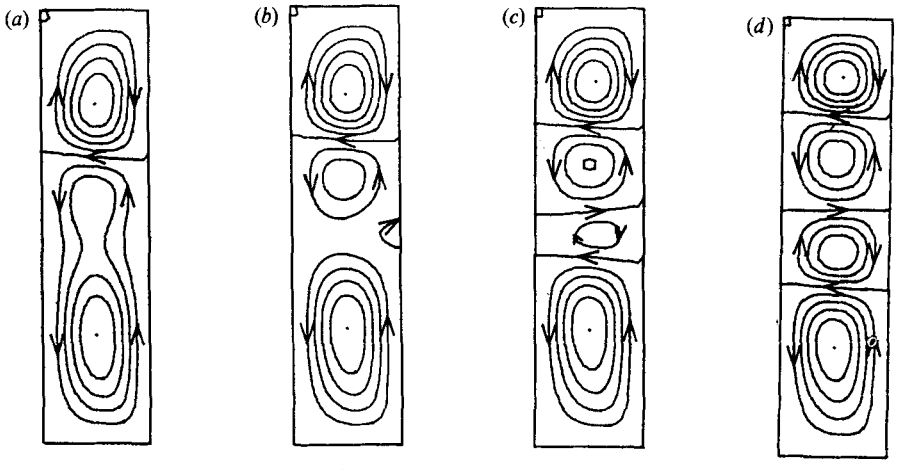

FIGURE 9. Transient development of 2–4 transition for buoyant flows, at $Re = 85$ and $\Gamma = 4.05$, with $Gr = 300$, (a) $Fo = 0$, (b) 1.24, (c) 1.86, (d) 6.19.

3.2. *The four-cell to six-cell transition*

As with the two-to-four cell transitions, the purpose of the first series of computations was to reproduce the available experimental results for the bifurcation set in the (Re, Γ)-plane for four-cell and six-cell flows, in order to validate the procedure used and to verify the accuracy of the results obtained. In figure 10, the experimental results of Mullin (1982) and Mullin *et al.* (1982) have been reproduced, and are compared with the finite-difference predictions made in this study. The same methods of determining the primary-flow locus as described in the previous section were used in this case. The agreement with the experimental results of Mullin is observed to be quite good, both quantitatively and qualitatively. In particular, both curves exhibit the same upward-pointing cusp. The cusp in the numerical studies is observed to be somewhat steeper, with its tip extending to approximately ($Re = 70$, $\Gamma = 5.65$), compared with the experimental cusp, whose tip is around ($Re = 85$,

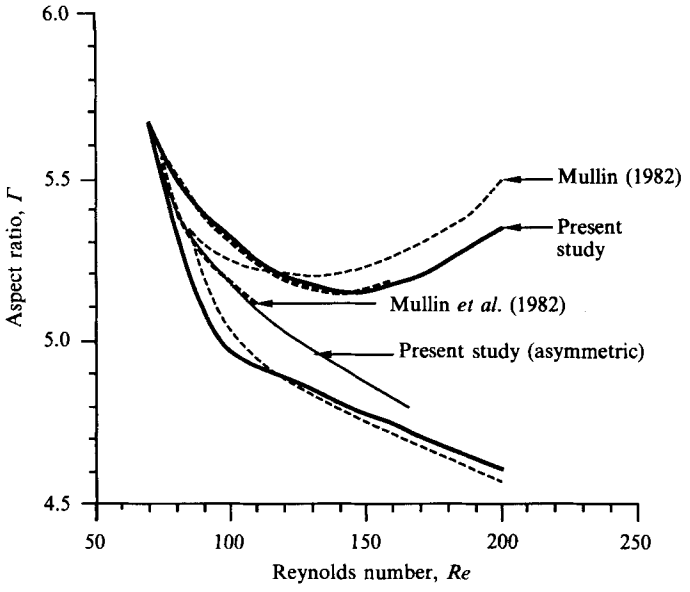

FIGURE 10. Bifurcation set for the isothermal ($Gr = 0$) four-cell and six-cell flows.

$\Gamma = 5.35$). The reason for this is that Mullin's data are for a radius ratio of $\eta = 0.6$, while the numerical study assumes $\eta = 0.5$. The effects of decreasing η on the flow have already been discussed in the previous section. It is also pointed out that these effects would be expected to diminish as Γ increases, since the length of each cell is a smaller percentage of the total annulus length, and adjustments from one particular pattern to another represent a less drastic change in the system. Another possible reason for this slight discrepancy is that the experimental measurements in the region of the cusp were quite sensitive (Mullin 1982), and the experimental system is subject to more uncontrollable disturbances and imperfections than a mathematical formulation. Thus, one would expect to obtain slightly lower stability limits for the secondary modes from a numerical study. Jones & Cliffe (1983) also found the cusp to be extended slightly in their numerical study, compared with the experimental case.

A more direct comparison with experimental data is obtained from the results of Mullin *et al.* who used a radius ratio of $\eta = 0.507$. The agreement with the numerical results along the upper portion of the locus is excellent. The experimental results along the bottom portion of the locus, however, show an earlier loss of stability and collapse of the six-cell secondary flow as the Reynolds number is decreased. To reconcile this discrepancy, a new set of critical values was determined along the lower portion of the locus using the quasi-static variation of Re at fixed Γ (in contrast to the impulsive technique described in §3.1). The locus determined in this way is shown in figure 10 as a thin solid line, and is observed to coincide with the experimental results. The reason for this shift in the locus is described below.

In the study by Cliffe (1988), it was observed that the six-cell secondary mode loses its stability, owing to asymmetric disturbances, at higher values of Re than those corresponding to the critical locus for symmetric flows. While the present study is not restricted to symmetric solutions, the development of the Taylor-vortex flow from an initial state of rest, with an impulsive start at a given value of Re, proceeds in a symmetric fashion from both ends (cf. Ball & Farouk 1987). In contrast, a quasi-

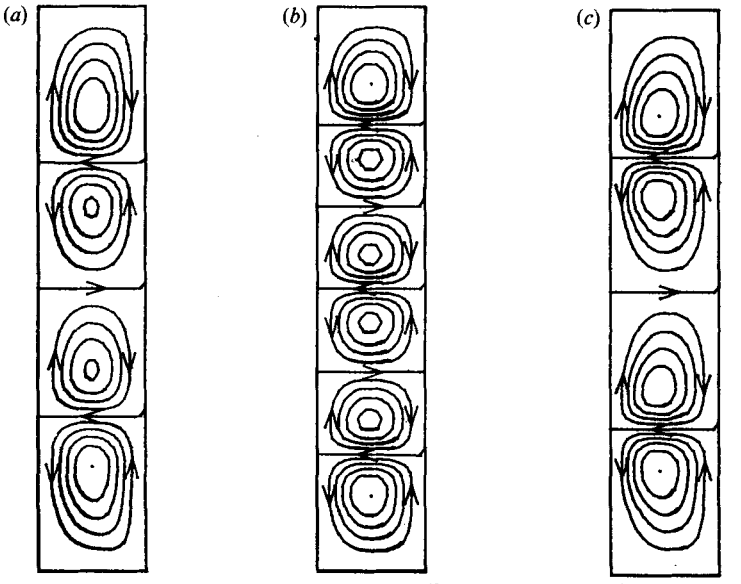

FIGURE 11. 4–6–4 Flow transition with increasing Re at $\Gamma = 5.2$, with $Gr = 0$, (*a*) $Re = 85$, (*b*) 140, (*c*) 200.

static reduction in Re would necessarily introduce asymmetric perturbations to the initial flow. This is a result of the interaction of an impulsive reduction in the speed of rotation of the inner cylinder with the established (steady-state) vorticity field, and is apparent by examining (9). Immediately after a quasi-static reduction in Re, the value of v^2/r will be reduced everywhere, perturbing the symmetry of the vorticity field through the $\partial/\partial z(v^2/r)$ production term.

Since the introduction of buoyancy into the Taylor experiment breaks the midplane symmetry of the system (Ball & Farouk 1987), no differences in the critical values of Re should be observed between the impulsive-start and the quasi-static variation methods for the mixed-convection runs.

In figure 11, streamlines are presented for the isothermal case ($Gr = 0$) with $\Gamma = 5.2$, for three different values of Re (85, 140, and 200). The point ($Re = 85$, $\Gamma = 5.2$) lies just to the left of the state locus in figure 10, ($Re = 140, \Gamma = 5.2$) lies just above the upper part of the locus near its relative minimum, and ($Re = 200, \Gamma = 5.2$) lies just below the upper part of the locus as it starts to increase again. Thus, $\Gamma = 5.2$ is observed to be in the region where the two modes exchange priorities, and as Re is decreased from $Re = 200$ at $\Gamma = 5.2$, the flow changes from a four-cell flow, to a six-cell flow, then back to a four-cell flow, as shown.

In figure 12, the effects of adding buoyancy to the system by heating the inner cylinder are examined. Shown in this figure are the loci for three fixed values of the Grashof number (again, the isothermal flow locus is reproduced from figure 10 to facilitate comparisons). As with the two–four transition, it is observed that even a relatively small amount of buoyancy has a significant effect on the behaviour of the flow and its exchange process. For a Grashof number of only $Gr = 25$, the locus is shifted substantially towards higher values of Γ and Re. This is especially evident along the upper part of the locus, where the slope is dramatically increased. Furthermore, the cusp is diminished in width, indicating a less distinct hysteresis behaviour. As the Grashof number is further increased, these effects become more dominant. Finally, at $Gr = 1000$, the cusp has become unobservable.

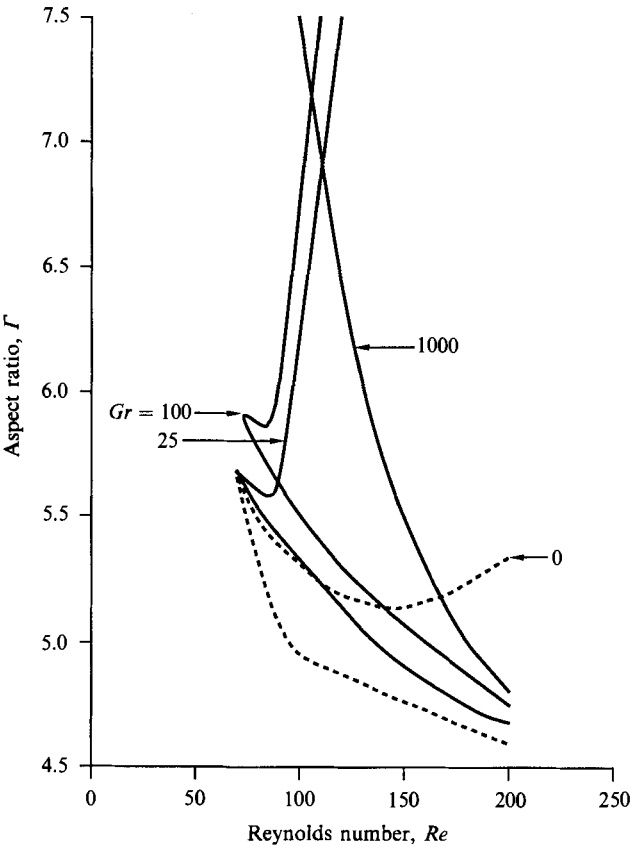

FIGURE 12. Bifurcation set for the buoyant four-cell and six-cell flows.

In figure 13, the change in the shape of the cusp with increasing buoyancy is explained by way of analogy with the codimension-2 unfolding of the pitchfork bifurcation, as was done in §3.1. In this case, however, the four-cell primary flow occurring at lower values of Γ is represented by the bifurcation diagram in the upper left region of the (α_1, α_2)-plane ($\alpha_1 > 0$ and $\alpha_2^3 < 27\alpha_1$), while the six-cell primary flow occurring at higher values of Γ is represented by the bifurcation diagram in the lower right region ($\alpha_1 < 0$ and $\alpha_2^3 > 27\alpha_1$). The curves in the (α_1, α_2)-plane joining these two regions as Γ is increased always pass to the left of the origin, as shown. As the buoyancy force is increased, the curves move further and further away from the origin, representing a growing imperfection in the system.

The mixed convection case $Gr = 100$ is shown in figure 14, for $\Gamma = 5.9$ and $Re = 70$, 80, and 120. These values are analogous to the results shown in figure 11, with the flow changing from four cells, to six cells, and back to four cells as Re is decreased. The buoyancy is observed to have little noticeable effect on the six-cell flow at $Re = 80$, but the four-cell flows are slightly distorted. The upper pair of cells in these cases is somewhat larger than the bottom pair, and in the case $Re = 70$, a large, stagnant region is present. In this region, the buoyancy is just strong enough to suppress the development of another pair of counter-rotating cells.

In the transitions to a higher number of cells in buoyant flows, it is observed that the new pair is formed by the nucleation of a negative cell near the middle of a positive cell having a relatively stagnant region. This was discussed in §3.1 with

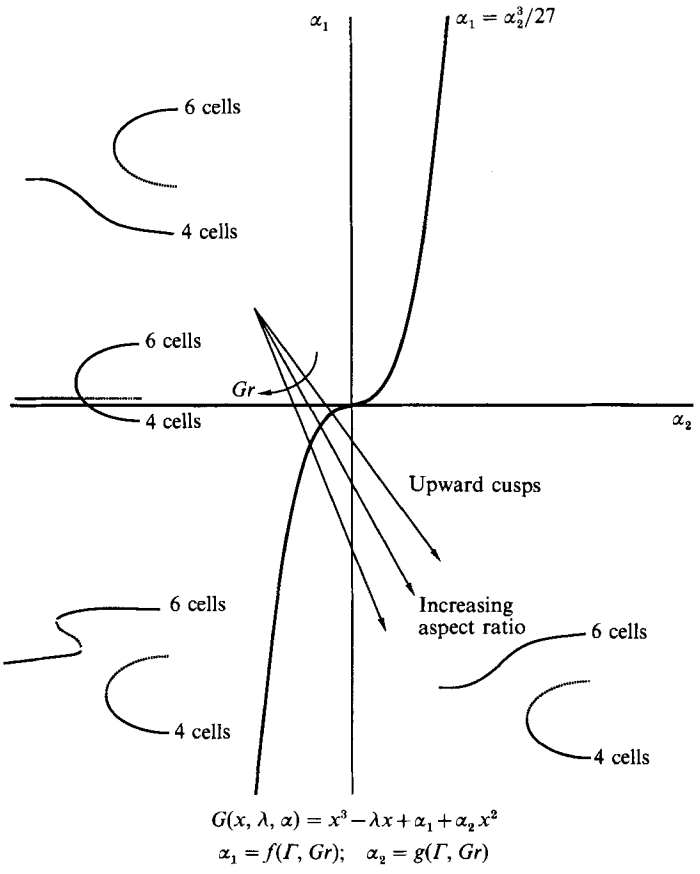

FIGURE 13. Unfolding of the pitchfork bifurcation: 4–6 cell exchange of priorities.

regards to the two–four transition. When comparing the two–four transition to the four–six transition, it is observed that the upper positive cell in the four-cell flow is the one to become unstable. Furthermore, both the negative and positive cells in the upper pair are extended in size as the transition is approached, while the lower pair remains essentially unchanged. This phenomenon can be explained by considering the temperature field which develops within the annulus. For this purpose, a four-cell flow and a six-cell flow are presented, together with their isotherms, for $\Gamma = 5.1$ with $Gr = 100$. The four-cell flow, shown in figure 15, is for $Re = 140$, while the six-cell flow in figure 16 is for $Re = 150$. These two flows bracket the critical value of Re for this aspect ratio and Grashof number.

In both of these figures, a noticeable distortion of the temperature field is observed, and is caused by the counter-rotating secondary flow. Consider figure 15, where there are two pairs of counter-rotating cells. The bottom cell is rotating in the counter-clockwise direction, while the cell immediately above it is rotating in the clockwise direction. Acting together, they transport the relatively hotter fluid near the heated inner cylinder out into the annular gap, creating a local temperature inversion just above the interface between the two cells. The same situation exists between the upper pair of cells.

Now, as the aspect ratio of the annulus is increased, the cells must adjust to fill the extra volume. One might assume that each cell would increase by an equal amount.

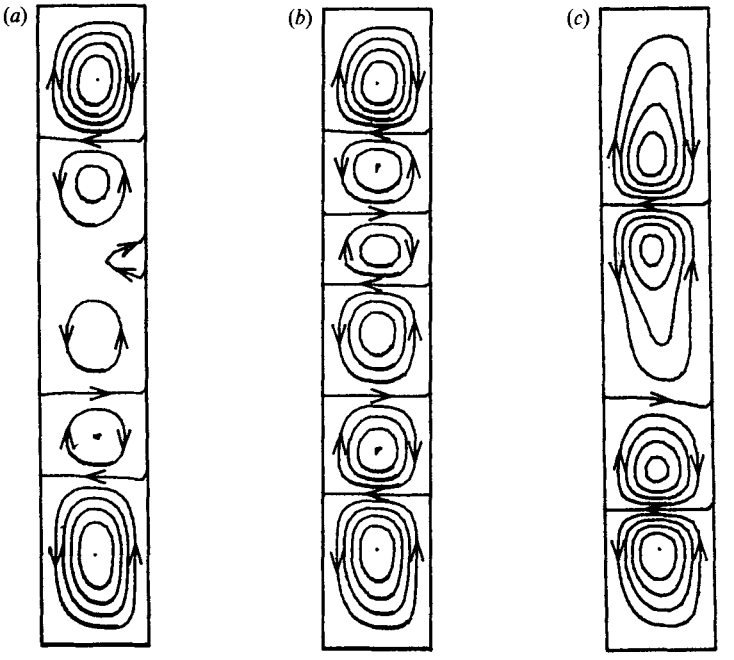

FIGURE 14. 4–6–4 Flow transition with increasing Re at $\Gamma = 5.9$, with $Gr = 100$, (*a*) $Re = 70$, (*b*) 80, (*c*) 120.

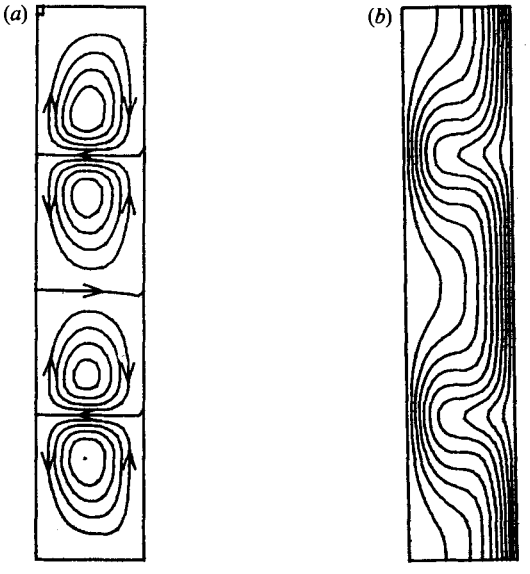

FIGURE 15. Buoyant four-cell flow for $Re = 140$, $Gr = 100$ and $\Gamma = 5.1$, (*a*) streamlines, (*b*) isotherms.

This is more or less the case for the isothermal flows. However, in the mixed convection flows, there exist unstably stratified fluid layers caused by the local temperature inversions. This unstable stratification is confined to the regions occupied by the negative Taylor cells. As a consequence of the tendency of an unstably stratified fluid layer to overturn, the negative cells tend to remain the same size.

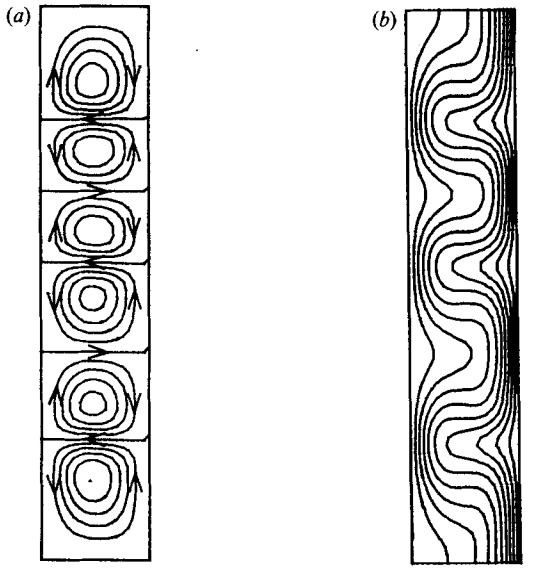

FIGURE 16. Buoyant six-cell flow for $Re = 150$, $Gr = 100$ and $\Gamma = 5.1$, (a) streamlines, (b) isotherms.

An analogy is made with the case of the Rayleigh–Bénard instability in thin fluid layers heated from below. The critical Rayleigh numbers for these flows are based on the depth of the fluid. As this depth is increased, the flows become less stable. The depth of the fluid layer is analogous to the volume occupied by the negative Taylor cells. From a thermal stability perspective, a smaller volume represents a more stable arrangement. In spite of this, when there are more than one negative Taylor cells, as in the four-cell flow, the uppermost cell is still observed to increase in size. For this cell, there is an additional consideration, namely, the presence of the upper stationary end. It is recalled that there is a contribution to the negative vorticity at the top of the annulus due to the Ekman layers (cf. Snyder & Lambert 1966). Also, the flow immediately adjacent to the ends is less vigorous than in the central part of the annulus. These two effects combine to lessen the thermal instability caused by the Taylor cells near the top of the annulus.

4. Conclusion

In the idealized Taylor-vortex problem, the annulus is assumed to be of infinite length. The resulting flow is periodic in the axial direction, and arises from symmetric supercritical bifurcations from the base flow. When a finite geometry is considered, the solutions generally cannot be periodic in z, and the symmetry of the problem is broken (Benjamin 1978*a*). Furthermore, the base flow is altered by the presence of the ends, where a no-slip boundary condition is enforced. This imperfection in the system leads to a folding of the primary-flow locus as the aspect ratio and Reynolds numbers are varied, and the exchange of the primary mode from one array of cells to another is accompanied by a hysteresis. This hysteresis is indicated by a cusp pointing obliquely to the Re-axis in the (Re, Γ)-control plane.

In this paper, the development of the primary flow as the aspect ratio is varied was investigated for both buoyant and isothermal flows, in order to ascertain the role of buoyancy in the bifurcation phenomena. Two different ranges of the aspect ratio

were studied, corresponding to the 2–4 and 4–6 cell transitions in the flow. For isothermal flows, the cusp characterizing the 2–4 cell transition pointed downward, while the 4–6 cell transition was characterized by an upward-facing cusp. When buoyancy was introduced to the system (by heating the inner cylinder), the downward facing cusp in the 2–4 cell transition began to align with the Re-axis. At $Gr = 100$, a pitchfork bifurcation was indicated, and then the cusp pointed upward as Gr was further increased. In both cases, as Gr was increased, the loci were shifted towards higher values of Γ. This shift was particularly large along the upper portion of each locus. Finally, the hysteresis of the flow was diminished with increasing Gr, as indicated by the width of the cusp. Indeed, at sufficiently high values of Gr, the cusp was unobservable.

The physical interpretation of the observed effects of buoyancy on the behaviour of these flows is difficult. The presence of buoyancy represents another imperfection in the system, as the action of the gravitational force is always vertically downward. Furthermore, as with the annulus ends, the buoyancy changes the base flow by inducing convective motion of the fluid. Different imperfections may change the bifurcation curves in different ways, and the mathematical theory cannot predict the behaviour of systems with more than one imperfection except in very general terms (Drazin & Reid 1984).

Despite these shortcomings of the theory, some insight to the effects of buoyancy on the bifurcation phenomena can be obtained by considering the actual behaviour of the flow. First, it has been observed that the presence of buoyancy tends to assist the Taylor cells whose direction of circulation is upward along the heated inner cylinder (Ball & Farouk 1986). As the aspect ratio is increased in a buoyant flow, the system adjusts to the increased volume by a growth in the size of those positive cells. By contrast, in the isothermal flow the adjustment is uniform in each counter-rotating pair of cells. Since the positive cells in the buoyant flows have been observed to remain stable at sizes of over three times the size of the negative cells (Ball 1987), the buoyancy clearly favours the Taylor-cell state with the lower number of cells. This results in an upward shift of the primary-flow locus.

Another consideration is the effect of the temperature gradient on the stability of the various cellular modes of flow. Local inversions of the temperature field exist in the neighbourhood of each negatively rotating cell, and these unstably stratified regions tend to suppress the growth of those cells, contributing to the increased stability of the lower-wavenumber flows. Finally, the negative temperature gradient across the annulus has a stabilizing effect on the flow, as the lighter fluid particles near the heated cylinder surface have a smaller centrifugal force exerted on them.

The use of a CRAY X-MP supercomputer was made possible by the National Science Foundation (Grant ECS-8515763). The authors appreciate the extremely thoughtful and helpful review provided by one of the referees. K. S. B. would also like to thank Dr Hüseyin Koçak for his helpful discussions on unfoldings.

REFERENCES

Andereck, C. D., Liu, S. S. & Swinney, H. L. 1986 Flow regimes in a circular Couette system with independently rotating cylinders. *J. Fluid Mech.* **164**, 155–183.

Astill, K. N. 1964 Studies of the developing flow between concentric cylinders with the inner cylinder rotating. *Trans. ASME* C: *J. Heat Transfer* **86**, 383–392.

Ball, K. S. 1987 Mixed convection heat transfer in rotating systems. Ph.D. thesis, Drexel University.

BALL, K. S. & FAROUK, B. 1986 Numerical studies of mixed convection flows in the annulus between vertical concentric cylinders with rotating inner cylinder. In *Proc. Eighth Intl Heat Trans. Conf. San Francisco* (ed. C. L. Tien, V. P. Carey & J. K. Ferrell), pp. 435–440. Hemisphere.

BALL, K. S. & FAROUK, B. 1987 On the development of Taylor vortices in a vertical annulus with a heated rotating inner cylinder. *Intl J. Num. Meth. Fluids* **7**, 857–867.

BECKER, K. M. & KAYE, J. 1962*a* Measurements of diabatic flow in an annulus with an inner rotating cylinder. *Trans. ASME* C: *J. Heat Transfer* **84**, 97–105.

BECKER, K. M. & KAYE, J. 1962*b* The influence of a radial temperature gradient on the instability of fluid flow in an annulus with an inner rotating cylinder. *Trans. ASME* C: *J. Heat Transfer* **84**, 106–110.

BENJAMIN, T. B. 1978*a* Bifurcation phenomena in steady flows of a viscous fluid. I. Theory. *Proc. R. Soc. Lond.* A **359**, 1–26.

BENJAMIN, T. B. 1978*b* Bifurcation phenomena in steady flows of a viscous fluid. II. Experiments. *Proc. R. Soc. Lond.* A **359**, 27–43.

BENJAMIN, T. B. & MULLIN, T. 1981 Anomalous modes in the Taylor experiment. *Proc. R. Soc. Lond.* A **377**, 221–249.

BENJAMIN, T. B. & MULLIN, T. 1982 Notes on the multiplicity of flows in the Taylor experiment. *J. Fluid Mech.* **121**, 219–230.

BETTES, T. 1982 Chemical vapor deposition, trends and equipment. *Semiconductor Intl, Denver.* March, 59–72.

BJORKLUND, I. S. & KAYS, W. M. 1959 Heat transfer between concentric rotating cylinders. *Trans. ASME* C: *J. Heat Transfer* **81**, 175–186.

BOLLEN, L. J. M. 1978 Epitaxial silicon, state-of-the-art. *Acta Electronica* **21**, 185–199.

CHOSSAT, P., DEMAY, Y. & IOOSS, G. 1985 Recent results about secondary bifurcations in the Couette–Taylor problem. *Fourth Taylor Vortex Flow Working Party, Karlsruhe.*

CHOSSAT, P. & IOOSS, G. 1985 Primary and secondary bifurcation in the Couette–Taylor problem. *Japan J. Appl. Maths* **2**, 37–68.

CLIFFE, K. A. 1983 Numerical calculations of two-cell and simple-cell Taylor flows. *J. Fluid Mech.* **135**, 219–233.

CLIFFE, K. A. 1988 Numerical calculations of the primary flow exchange process in the Taylor problem. *J. Fluid Mech.* (In press.)

CLIFFE, K. A. & MULLIN, T. 1985 A numerical and experimental study of anomalous modes in the Taylor experiment. *J. Fluid Mech.* **153**, 243–258.

DEMAY, Y. & IOOSS, G. 1984 Calcul des solutions bifurquées pour le probléme de Couette–Taylor avec les deux cylindres en rotation. *J. Méc. Théor. Appl. Numéro Spécial*, pp. 193–216.

DE VAHL DAVIS, G., LEONARDI, E. & REIZES, J. A. 1984 Convection in a rotating annular cavity. In *Heat and Mass Transfer in Rotating Machinery* (ed. D. E. Metzger & N. H. Afgan), pp. 131–142. Hemisphere.

DIPRIMA, R. C. & SWINNEY, H. L. 1985 Instabilities and transition in flow between concentric rotating cylinders. In *Hydrodynamic Instabilities and the Transition to Turbulence*, 2nd edn (ed. H. L. Swinney & J. P. Gollub), pp. 139–180. Springer.

DRAZIN, P. G. & REID, W. H. 1984 *Hydrodynamic Stability.* Cambridge University Press.

FUNG, Y. T. & KURZWEG, U. M. 1975 Stability of swirling flows with radius dependent density. *J. Fluid Mech.* **72**, 243–255.

GARDNER, S. R. M. & SABERSKY, R. H. 1978 Heat transfer in an annular gap. *Intl J. Heat Mass Transfer* **21**, 1459–1466.

GAZLEY, C. 1958 Heat transfer characteristics of the rotational and axial flow between concentric cylinders. *Trans. ASME* C: *J. Heat Transfer* **80**, 79–90.

GOLUBITSKY, M. & SCHAEFFER, D. G. 1985 *Singularities and Groups in Bifurcation Theory*, vol. 1. Springer.

GOSMAN, A. D., PUN, W. M., RUNCHAL, A. K., SPALDING, D. B. & WOLFSTEIN, M. W. 1969 *Heat and Mass Transfer in Recirculating Flows.* Cambridge University Press.

GREENSPAN, H. P. 1968 *The Theory of Rotating Fluids.* Cambridge University Press.

HALL, P. 1980 Centrifugal instabilities in finite containers: a periodic model. *J. Fluid Mech.* **99**, 575–596.

HALL, P. 1982 Centrifugal instabilities of circumferential flows in finite cylinders: the wide gap problem. *Proc. R. Soc. Lond.* A **384**, 359–379.

HOLMAN, J. P. 1981 *Heat Transfer*. McGraw-Hill.

HUGHES, C. T., LEONARDI, E., DE VAHL DAVIS, G. & REIZES, J. A. 1985 A numerical study of the multiplicity of flows in the Taylor experiment. *Phys. Chem. Hydrodyn.* **6**, 637–645.

JONES, I. P. & CLIFFE, K. A. 1983 Numerical studies for the flow due to rotating cylinders and disks. In *Proceedings of the Fifth Workshop on Gases in Strong Rotation, Charlottesville, Virginia* (ed. H. G. Wood), pp. 223–246.

KARLSSON, S. K. F. & SNYDER, H. A. 1965 Observations on a thermally induced instability between rotating cylinders. *Ann. Phys.* **31**, 314–324.

KAYE, J. & ELGAR, E. C. 1958 Modes of adiabatic and diabatic fluid flow in an annulus with an inner rotating cylinder. *Trans. ASME* C: *J. Heat Transfer* **80**, 753–765.

KREITH, F. 1968 Convection heat transfer in rotating systems. In *Advances in Heat Transfer*, vol. 5 (ed. T. F. Irvine & J. P. Hartnett), pp. 129–250. Academic.

LEONARDI, E., REIZES, J. A. & DE VAHL DAVIS, G. 1982 Heat transfer in a vertical rotating annulus – a numerical study. In *Proc. 7th Intl Heat Transfer Conf.* Paper no. FC12.

LORENZEN, A. & MULLIN, T. 1985 Anomalous modes and finite-length effects in Taylor–Couette flow. *Phys. Rev.* A **31**, 3463–3465.

MULLIN, T. 1982 Mutations of steady cellular flows in the Taylor experiment. *J. Fluid Mech.* **121**, 207–218.

MULLIN, T., PFISTER, G. & LORENZEN, A. 1982 New observations on hysteresis effects in Taylor–Couette flow. *Phys. Fluids* **25**, 1134–1136.

PATANKAR, S. V. 1980 *Numerical Heat Transfer and Fluid Flow*. Hemisphere.

SCHAEFFER, D. G. 1980 Qualitative analysis of a model for boundary effects in the Taylor problem. *Math. Proc. Camb. Phil. Soc.* **87**, 307–337.

SINGER, P. H. 1984 Techniques of low pressure chemical vapor deposition. *Semiconductor Intl, Denver*. May, 72–77.

SNYDER, H. A. 1965 Experiments on the stability of two types of spiral flow. *Ann. Phys.* **31**, 292–313.

SNYDER, H. A. & KARLSSON, S. K. F. 1964 Experiments on the stability of Couette motion with a radial thermal gradient. *Phys. Fluids* **7**, 1696–1706.

SNYDER, H. A. & LAMBERT, R. B. 1966 Harmonic generation in Taylor vortices between rotating cylinders. *J. Fluid Mech.* **26**, 545–562.

STREETT, C. L. & HUSSAINI, M. Y. 1987 A numerical simulation of finite-length Taylor–Couette flow. *AIAA Paper* 87-1444.

WALOWIT, J., TSAO, S. & DIPRIMA, R. C. 1964 Stability of flow between arbitrarily spaced concentric cylindrical surfaces, including the effect of a radial temperature gradient. *Trans. ASME* E: *J. Appl. Mech.* **31**, 585–593.

WAN, C. C. & CONEY, J. E. R. 1982 An experimental study of diabatic spiral vortex flow. *Intl J. Heat Fluid Flow* **3**, 31–38.

WITHJACK, E. M. & CHEN, C. F. 1974 An experimental study of Couette instability of stratified fluids. *J. Fluid Mech.* **66**, 725–737.